

Multi-Characteristic Parameter Classification Algorithm of Cracks on Bridge Substructures

Xiaoqiang Jia^{1,*} and Yidong Huang²

¹School of Computer Science, Weinan Normal University, Weinan, Shaaxi, 714099, China

²School of Science and Environmental Studies, Lakehead University, Ontario, Thunder Bay, P7B5E1, Canada

Received 3 December 2019; Accepted 14 March 2020

Abstract

The forms of bridge cracks vary widely, but the automatic classification and identification of the effects of these cracks are difficult to achieve. Many recognition systems developed all over the world are based on recognition results and carry out human-machine dialogues. These systems rely on the manual recognition of crack types, but the manual approach not only has a low working efficiency but also a high error rate. In this study, a classification algorithm for cracks on bridge substructures based on multi-characteristic parameters was proposed to accurately identify cracks on concrete bridges and objectively and accurately evaluate the state of the bridge cracks. The geometric characteristics of the cracks in the substructure were extracted, and the projection vector, crack area, distribution density, and Euler number were obtained. Projection and wavelet denoising algorithms were used to first distinguish the linear cracks from the network cracks, and the number of holes in the crack image was employed as a parameter to further determine the crack type. Then, the Euler number was introduced to retain the image characteristic when the image required to be changed. Finally, the back propagation (BP) neural network system was used to achieve an accurate crack classification. This study was verified by experiments. Results demonstrate that the classification algorithm can effectively identify four types of cracks, namely, transverse, longitudinal, reflective, and meshed cracks. In the identification of transverse, longitudinal, and reflective cracks, the corresponding classification accuracies in this study were 12%, 3%, and 4% higher than the classification algorithm with the canny operator. This study can meet the requirements of crack classification accuracy in practical engineering and provide a scientific reference for the maintenance of bridges.

Keywords: Crack image, Characteristic parameters, Euler number, Back propagation neural network

1. Introduction

The most common manifestation of early diseases of reinforced concrete bridges is the appearance of visible cracks, while the final adverse performance of other bridge diseases is usually attributed to the appearance of unacceptable cracks. Therefore, a timely detection of the occurrence and expansion of cracks on concrete bridges is important in effectively reducing the disease status of bridges and its influence. The classification of crack targets on concrete bridges is difficult and thus has become the key point of bridge-crack identification research. Only by accurately classifying bridge cracks can the crack parameters be further extracted, after which the state of the bridge cracks can be objectively and accurately evaluated. This scheme further indicates that a highly scientific and accurate basis for bridge maintenance should be provided. Scientific and effective bridge maintenance is achieved by conducting a reasonable method to evaluate the bridge's structure and by selecting a comprehensive inspection approach. However, due to the insufficient accuracy of conventional inspection methods, the damage caused during detection is usually large, which renders the detection work somewhat ineffective. Many accidents consequently occur, as bridge maintenance cannot be timely and effectively implemented.

In view of the abovementioned limitation, crack

recognition algorithms represented by neural network systems have become the mainstream topic in the field in recent years. Huang et al. [1] proposed an algorithm based on a fuzzy filter to extract the image characteristic vectors of cracks in a substructure, and then the crack types were identified using an artificial neural network. In the domain of crack recognition algorithms, Xiao et al. [2] adopted a moment invariant as the image characteristic of the crack and used a moment characteristic vector for description. Lins and Givigi [3] refined the target area of a crack image and extracted the intersection point of a skeletonized crack target, and then the perimeter and the number of the crack area were used to describe the crack image.

The above methods focus on crack target areas, but the calculation of the eigenvalue required by these methods is complicated, and the results eventually cannot meet relevant requirements. The classification accuracy of the traditional artificial measurement method is accompanied by a time-consuming and laborious process. Moreover, existing crack detection systems have low detection efficiency and poor measurement precision. Consequently, improving the classification efficiency and classification accuracy of bridge cracks has become an urgent endeavor.

Based on the above analysis, this study adopts the method of extracting the geometric characteristics of cracks in substructures and uses the neural network to classify the cracks. The aim is to construct a crack identification method that is as suitable for different conditions as possible. The accurate identification of transverse, longitudinal, meshed,

*E-mail address: xqjia@126.com

ISSN: 1791-2377 © 2020 School of Science, IHU. All rights reserved.

doi:10.25103/jestr.132.15

and reflective bridge cracks can help in the rapid and accurate evaluation of road conditions and provide a highly scientific reference for the maintenance of bridges.

2. State of the art

Cracks can only be classified if they are extracted. The extraction of cracks on a bridge requires an extraction of the crack edge of the bridge image and a description of the data structure. He et al. [4] proposed the use of the histogram analysis algorithm, in which the gray histogram of an image containing the crack area is assumed to have double peaks, and then a threshold was determined to split the crack image. This method is generally suitable for images with obvious cracks [5]. Li et al. [6] proposed the sobel edge detection algorithm and assumed that the perimeter pixel of the noise area is less than 20, whereas that of the crack area is greater than 20, then a threshold was used to remove the noise and obtain the crack segmentation image. However, due to the complex characteristic of the collected images for bridge cracks, the single fixed threshold was insufficient for the efficient splitting of the images. Grivas et al. [7] discussed a regional growth technology to split crack images, while Yan et al. [8] adopted a mathematical morphology to identify crack targets. However, as their algorithms did not consider the geometric correlation of crack images, their application scope was limited. Linsa et al. [9] employed a fuzzy segmentation method for crack images, in which the main idea was to set the pixels' gray value [10] in the crack image region smaller than that in the non-crack image region, hence ensuring continuity. In this scheme, a membership function for the image pixels' gray value to be obtained by a differential operation was utilized. Then, the parametric value was determined by using a genetic algorithm, and the target of the crack image was blurred. Finally, the crack image was split by connecting the pixels in the crack area according to their continuity characteristics. The artificial population algorithm [11] was a crack recognition algorithm widely searched at present, whose principle was based on the use of binary organisms, and operationalized by dividing images into blocks with different sizes. The deviation between the pixels' gray value and the pixels' gray mean value was calculated by using the sub-blocks as a means to obtain the crack area. This method could achieve a certain recognition effect, but its calculation was extremely large and hence limited in engineering applications. Zhu et al. [12] used the four basic operations of mathematical morphology (corrosion, expansion, and open and close operations) to handle linear crack targets. This method, which required crack targets to have a strong edge and multiple thresholds to be set, can reduce the availability and recognition effect.

Other image segmentation algorithms include the statistical filtering, cell unit, and texture analysis algorithms. The parametric description of crack image regions was usually based on moment descriptors. Jovisa et al. [13] adopted the Hu moment invariant to describe an image. Gishkori et al. [14] used the zernike moment invariant as the image characteristic to describe a crack. Qian et al. [15] refined the highway disease target and utilized the extracted skeletal bridge crack intersection, the perimeter of the crack area, and the area itself as a characteristic parameter to describe the crack image. The commonly used crack classifiers were the Bayesian [16-17], linear, and nonlinear classifiers [18]. Owing to the variety of bridge cracks and the difficulty of describing the degree of cracks with a

unified analytic formula, the topic on nonlinear classification algorithms based on artificial neural networks has become popular in the research of automatic recognition of bridge cracks. Sakshi et al. [19-21] studied the above classifiers and neural network classifiers and determined that neural network classifiers were significantly better than traditional classifiers.

The common problem of the abovementioned algorithms is that they can only derive a good recognition effect for a single crack, but they have a poor recognition effect for complex meshed cracks and block cracks. Thus, the application of such methods is greatly limited. Our present study, which is based on the geometric characteristics of cracks, including the projected area, distribution density, number of holes in the crack image, and the Euler number of the image, employs a neural network classifier to uniformly classify transverse, longitudinal, meshed, and reflective cracks. Projection variance and wavelet denoising are used to determine the transverse and longitudinal cracks. The ratio of the total number of crack pixels to the total number of crack pixels in the rectangular area surrounding the crack in the image is calculated. The results indicate that the distribution density of linear cracks (transverse and longitudinal cracks) is small, the distribution density of reflective cracks is large, and the distribution density of network cracks is the largest. When the image scale is changed and the crack of the adjacent pixels is used to calculate the Euler number, the projection variance, pixel distribution density of the crack area, Euler number, number of holes (such as the meshed cracks' target edge area surrounded by pixels) are combined to determine the crack types. The number of holes of the linear cracks is less than or equal to 1, whereas the number of holes of reflective and meshed cracks are greater than 1. Moreover, the number of holes of the reflective cracks is much lesser than that of the meshed cracks given the same image per unit area.

The remainder of this study is organized as follows. Section 3 describes the characteristics of the four types of cracks with different geometric shapes, and discusses the method of extraction of the projected areas and the distribution densities of the cracks. In this section, the number of image holes is used as a parameter for further identifying the types of cracks, then the images of the cracks on the bridge substructure are further classified using a classifier based on the back propagation (BP) neural network. Section 4 presents the analysis of the experimental results and discusses the variations in the calculation error with the increase in distance. Section 5 concludes the study, highlights the shortcomings of the research, and offers future research prospects.

3. Methodology

In this study, a classification algorithm based on the back propagation neural network is proposed for cracks on bridge substructures. In the proposed algorithm, Multi-characteristic parameters were obtained, including the projection vector, crack area, distribution density and Euler number. This section will present a detailed description of the proposed algorithm.

3.1 Crack-type analysis of bridge substructures

Asphalt concrete is mainly applied to the construction of high-grade highway bridges. The design life of concrete bridges is approximately 15 years. In long term usage, the

asphalt concrete bridges will gradually manifest various damages. Some parts of bridges on local roads can be damaged in less than two years. The damages, which appear as cracks, loose material, drifting, or water damage, will directly affect the service life of the bridge. Among them, cracks (the focus of this study) are the most common damage pattern in asphalt concrete bridges. Bridge cracks can be divided into four kinds based on their geometric characteristics, namely, transverse, longitudinal, meshed, and reflective cracks.

3.1.1 Transverse crack

Transverse cracks are caused by improper a degree inclination during roadbed compaction, i.e., the direction of inclination is nearly perpendicular to the center line of the bridge. Eventually, cracks will run through some parts or the entire bridge, and the widths will vary. Cracks develop at regular intervals. The semi-rigid base material, the crack resistance of the asphalt surface, and local temperature can determine the size of a crack gap. Transverse fractures are caused by numerous reasons, but the most common is temperature shrinkage cracking, in which the asphalt can neither meet the quality standards fit for local climatic conditions nor the operating requirements. Asphalt surface shrinkage caused by temperature or temperature fatigue stress is much larger than the tensile strength of the asphalt mixture. Moreover, cracks are caused by the shrinkage of the semi-rigid base. During construction, damage occurs when cracks are not buried properly or when joints are not positioned closes enough to result in a poor bonding. An image of a typical transverse crack is shown in Fig.1 (a).

3.1.2 Longitudinal cracks

The formation of longitudinal cracks is the same as that of transverse cracks; that is, the direction is nearly parallel to the driving direction, with varying lengths and widths. Longitudinal cracks are mainly concentrated in crowded places or driveways. For instance, traffic on a highway is clearly channelized, and the position of wheel tracks and the range of distribution are both small. Moreover, all kinds of vehicles are mostly concentrated on driveways. Longitudinal cracks develop at the center of these driveways or near the marking lines. The width of the slit is usually 5-10 mm, the length is from tens to hundreds of meters, and the fractures appear as a single crack. Two reasons can help explain the occurrence of longitudinal cracks. First, when the asphalt surface is paved according to road width, the stubble between these two elements cannot be effectively handled, and cracks gradually develop under the influence of atmospheric factors and vehicle loads. The second reason can be explained by uneven settlement caused by rainwater erosion or uneven compaction at the edges of bridge foundations. Fig.1 (b) shows an image of a typical longitudinal crack.

3.1.3 Irregular meshed cracks

Rainwater, particularly large amounts of precipitation, infiltrates and remains on the surface and middle layers of highways. Fast driving can cause asphalt layers on the gravel of the asphalt concrete to peel off, resulting in irregular meshed cracks on highway surfaces. These cracks appear as crisscrossed cracks with slit widths of at least 1 mm, slit distances not exceeding 40 cm, and slit areas of at least 1 m². The formation of meshed cracks is caused and accelerated by weak or marl layers sandwiched in the bridge structure, loose granular layers and poor water stability, poor quality

of the asphalt and low ductility of the mixture, poor crack resistance, insufficient thickness of the asphalt layer, interlayer adhesion with poor junction, and infiltration of water. The overall strength of the bridge is eventually weakened, and meshed cracks are formed in the early stages, manifesting as bridge cracks. Subsequently, the cracks gradually expand, and the gaps between cracks are decreased. Meshed cracks are serious types of cracks. Fig.1(c) shows a typical image of a meshed crack.

3.1.4 Reflective cracks

When the foundation layer of a highway bridge develops cracks, these cracks will gradually affect the asphalt bridge under the influence of various factors. The position and shape of the bridge cracks are nearly the same as those of the base cracks. Reflective cracks are mainly caused by the uneven settlement of soft base sections, which is directly reflected on the asphalt bridge. Fig.1. (d) shows an image of a reflective crack.

The final parameters need to extract the different points of four kinds of cracks. Crack length, width, and other information need to be extracted as the parameters for transverse and longitudinal cracks, whereas crack area, width, and shape information need to be extracted as the parameters for meshed cracks. Thus, the first problem of this study is determining how to use the image recognition method to classify the lower-structural cracks.

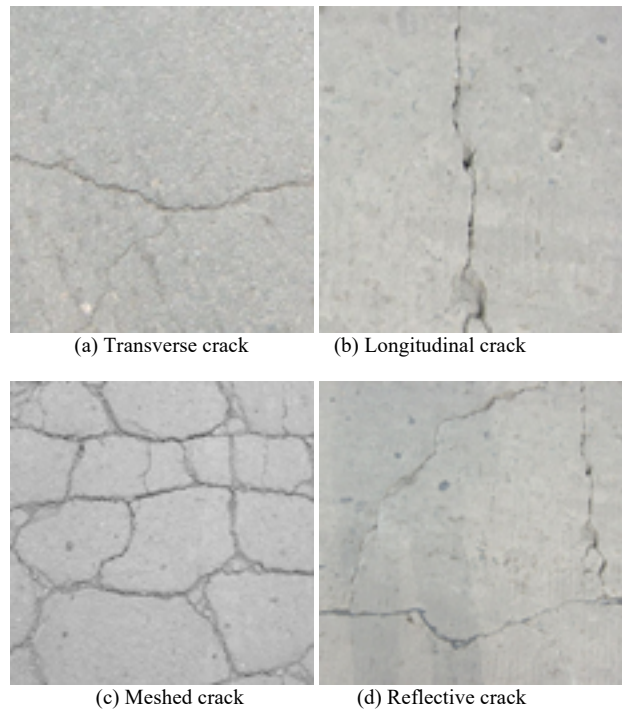


Fig. 1. Four types of cracks

3.2 Differences in the projection characteristics of linear and irregular meshed cracks

The x directions and y directions of a projection were separately considered for the different types of crack images of a bridge foundation. If the cracks are relatively serious, then the projections of the x directions and y coordinates will increase considerably. The directionalities of the transverse and longitudinal cracks are strong. By contrast, the block and meshed cracks are evenly distributed in the bridge image, but they have weak directionalities, with relatively large projections on the directions x and y coordinates. The type and extent of bridge cracks can be

identified according to the direction and size of the projection. First, the linear cracks were distinguished from the irregular meshed cracks. Then, the transverse and longitudinal cracks were determined by using the combined projection property and wavelet denoising method. The process flow employed in this study is shown in Fig.2.

For a standard transverse crack, the projection of the y axis produces an obvious peak value, while the projection waveform of the x axis is even. As for the standard longitudinal crack, the projection on the x axis produces an obvious peak, while the projection on the y axis waveform is even. Irregular transverse and longitudinal cracks with tilt angles of 45° are called oblique cracks. As crack targets are generated at a certain angle, the corresponding projections on the directions x and y axes appear with a rising trend. However, due to energy dispersion, no jump peaks are expected, as the waveform is relatively flat on the x directions and y axes. Subsequently, according to such projection characteristics, linear and irregular network cracks can be distinguished, but it is still not effective for the oblique and meshed cracks

The projection signal is expected to be a mix of small values in the noise signals. The complexity of judging projection peaks based on statistical projections is simplified by finding a threshold and using a one-dimensional wavelet transform for the denoising. Then, normalization is performed until the type of crack can be finally distinguished based on the characteristics of the projection's curve peaks.

3.2.1 Algorithm steps for crack determination

The binarization image [22-23] I was derived from the image segmentation process. The pixel value of the crack target is set equal to 1, and the pixel point of the perfect road background is set to 0. The projection vectors of x and y of the binarization image I was calculated in the horizontal and vertical directions, respectively.

$$x(i) = \sum_{j=1}^M I(i, j) \tag{1}$$

$i=1,2,\dots,N$

$$y(j) = \sum_{i=1}^M I(i, j) \tag{2}$$

$j=1,2,\dots,N$

Then, a projection operation was implemented for the crack images. For a standard transverse crack, the projection vector of the y coordinates will have a distinct wave peak, while the projection waveform of the x coordinates will be uniform without any prominent wave peak (Fig.3 (a)). For a standard longitudinal crack, the projection vector of the x coordinates will have an obvious wave peak, while the projection waveform of the y coordinates will be uniform without any prominent peak. For the meshed and reflective cracks, given their irregular segments in different directions, the projection of the x coordinates and y coordinates will have multiple prominent peaks (As shown in Fig.3 (b)).

Subsequently, a difference operation was rendered for the projection sequences of $x(i)$ and $y(j)$ as a means to derive the absolute value accumulation of the difference:

$$Q_s = \sum_{i=1}^M |x_s(i+1) - x_s(i)| y(j) \tag{3}$$

$$Q_t = \sum_{j=1}^M |Y_t(j+1) - Y_t(j)| \tag{4}$$

Q_s and Q_t were used to reflect the characteristics of the multidirectional crack seam and the parametric distribution. The greater the eigenvalue is, the greater the sum of the absolute value will be for the projection differences of the crack images on a given direction. Q_t is markedly greater than Q_s for the transverse cracks, whereas Q_s is considerably greater than Q_t for the longitudinal cracks. For meshed and reflective cracks, Q_s is approximated by Q_t . Thus, projection differences can effectively distinguish the transverse and longitudinal cracks but not the meshed and reflective cracks.

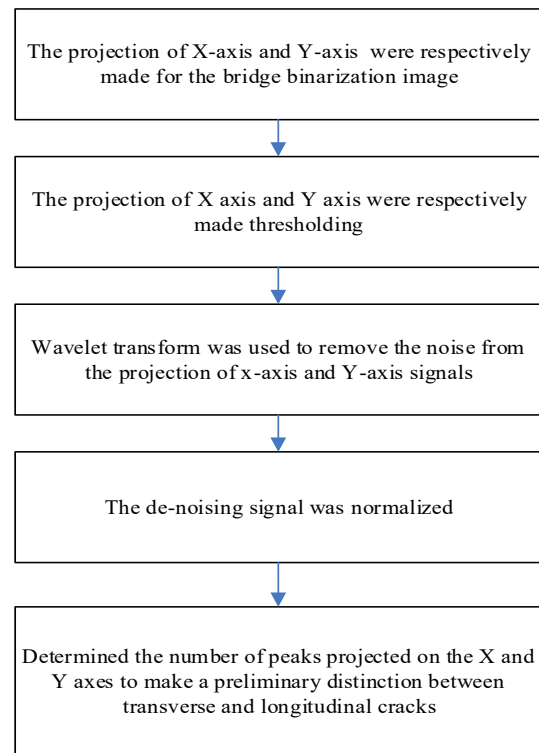
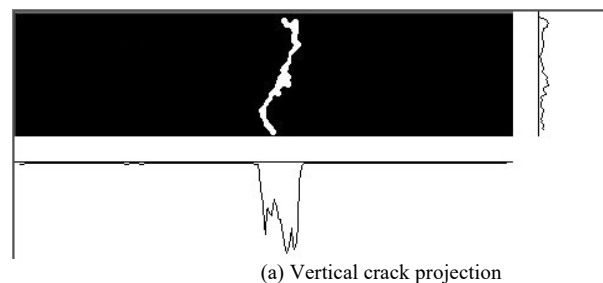
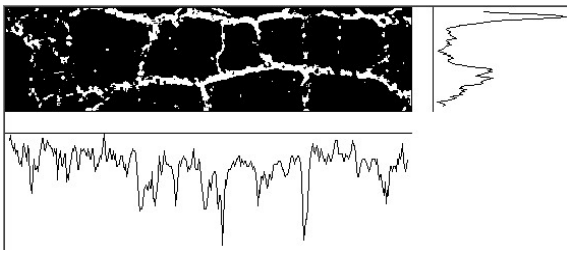


Fig.2. Flow of the lower-substructure crack classification algorithm



(a) Vertical crack projection

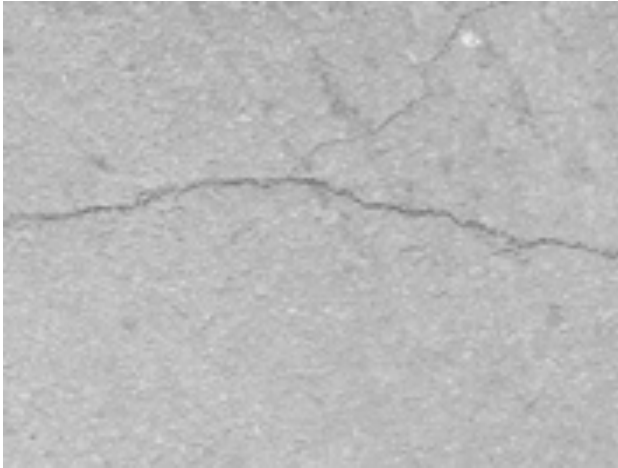


(b) Cross crack projection

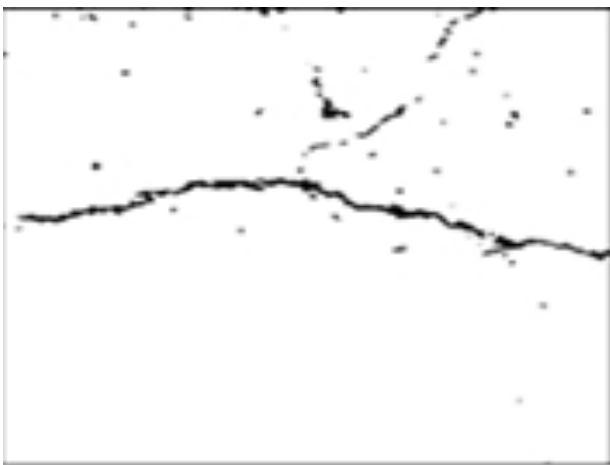
Fig.3. Operation of the projection vector

3.2.2 Experimental results

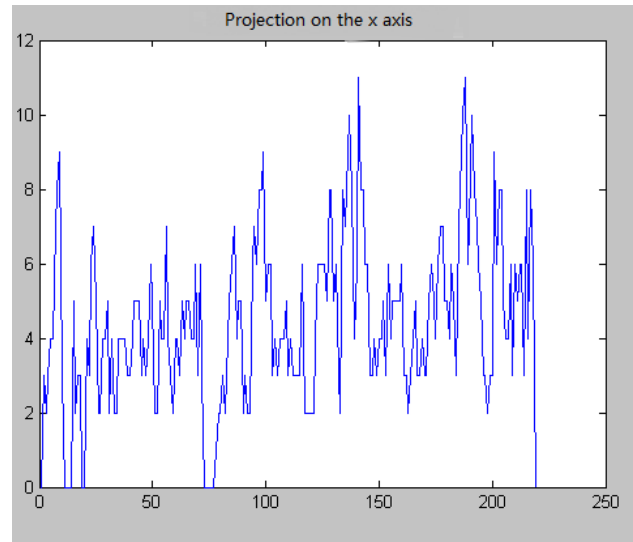
The method discussed above was used to carry out the experiments. The results are shown in Fig.4 (a) - (f).



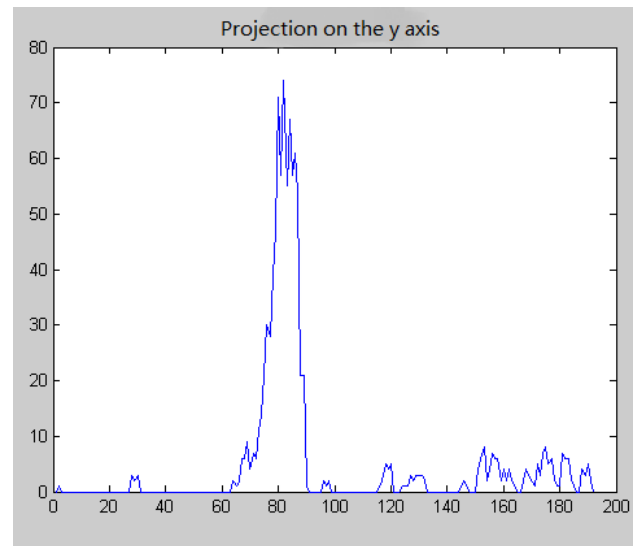
(a) Original image of the transverse crack



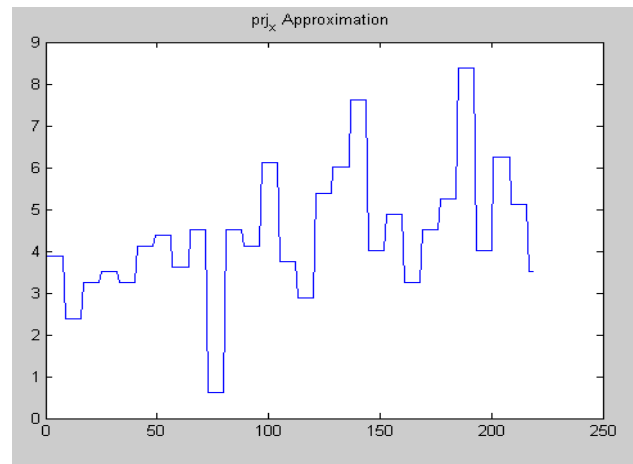
(b) Binary image



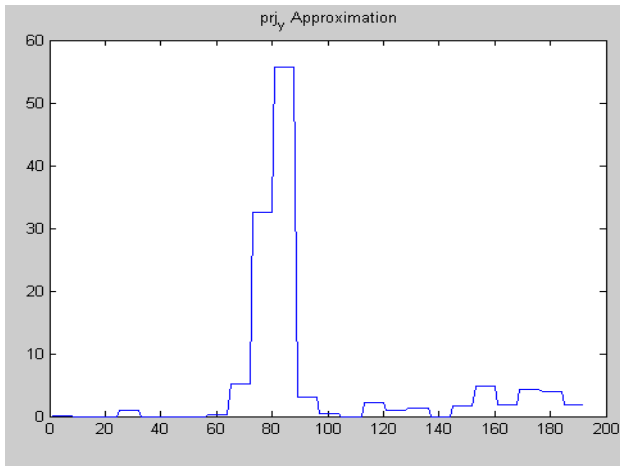
(c) Projection on the x axis



(d) Projection on the y axis



(e) Wavelet denoising signal of the projection threshold on the x axis



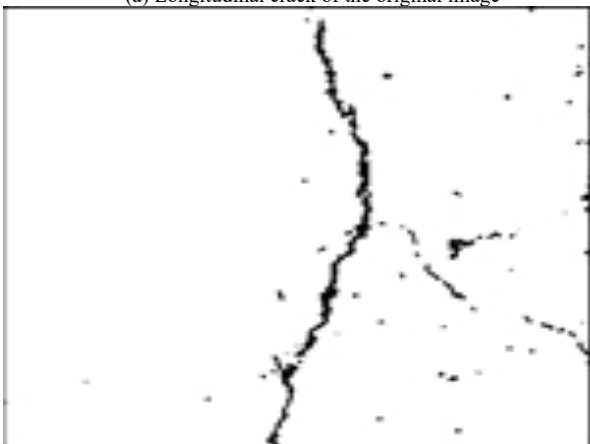
(f) Projection threshold on the y axis after a wavelet denoising of the signal

Fig. 4. Classification method of the transverse crack

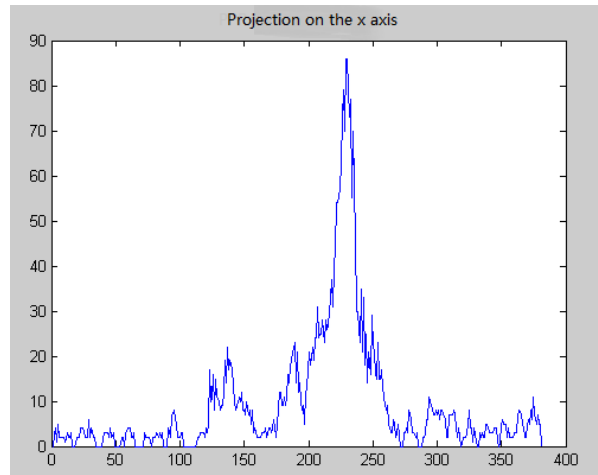
Fig.4 (a) shows a sample of the bridge image's transverse cracks. As shown in Fig.4 (f), the projection of the y coordinate has an obvious peak with a value of approximately 56, and its position coincides with that corresponding to the cracks in the original image. The change in the projection of the x coordinates is relatively uniform, and the projection quantity is small at less than 12.



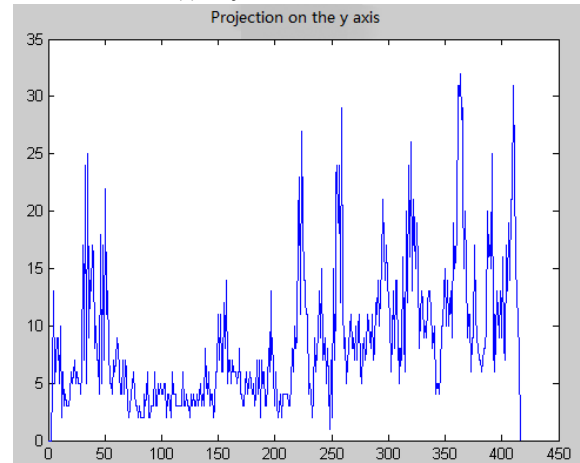
(a) Longitudinal crack of the original image



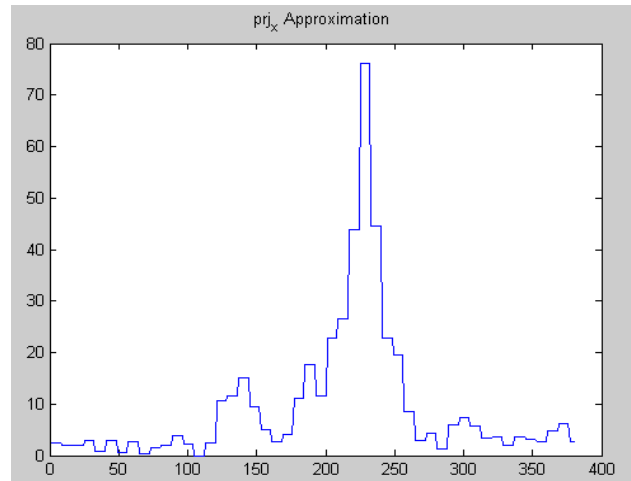
(b) Binary figure



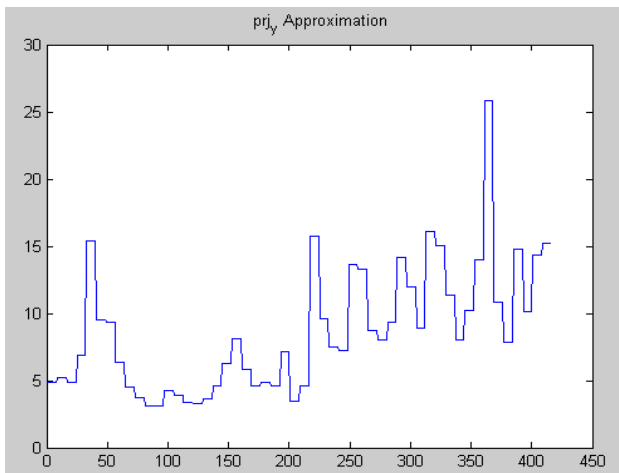
(c) Projection on the x axis



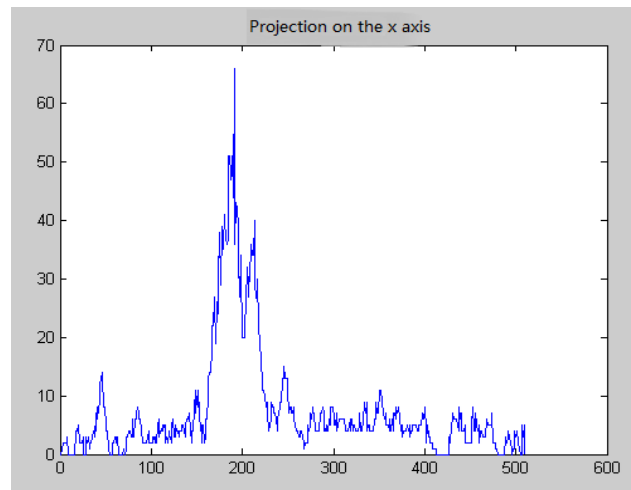
(d) Projection on the y axis



(e) Projection on x after wavelet denoising



(f) Projection on y axis after wavelet denoising



(c) Projection on the x axis

Fig.5. Case diagrams of the longitudinal fracture classification method

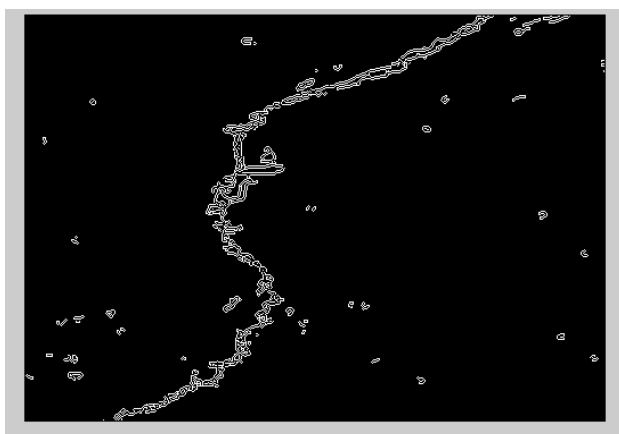
Fig.5 (a) presents an image of a longitudinal crack. As shown in Fig.5 (e), the projection of the x coordinates has an obvious peak, whereas that of the y coordinates changes more evenly. Fig.6 (a) shows another longitudinal crack, and the derived results are the same as those in Fig.5.

The projection of the y coordinates was set with a threshold and denoised by the wavelet transform, as shown in Fig.6 (f).

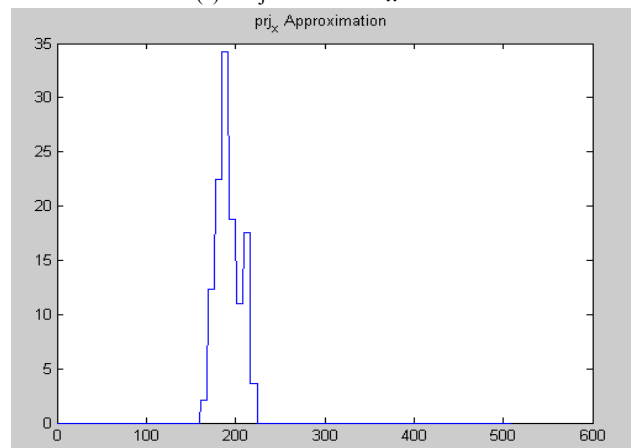
Subsequently, the classification method is analyzed, and the steps for the meshed cracks were implemented.



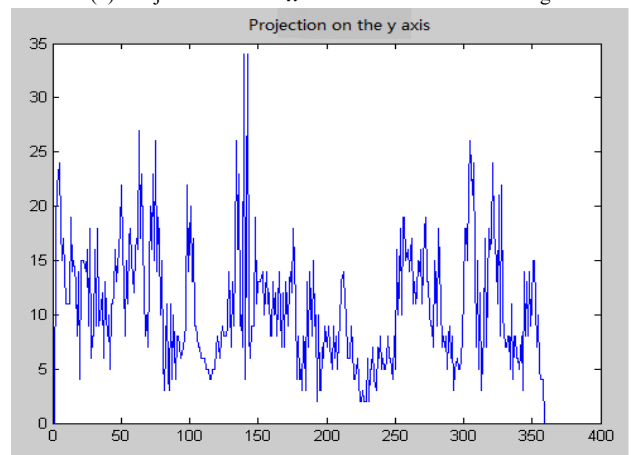
(a) Longitudinal cracks of the original image



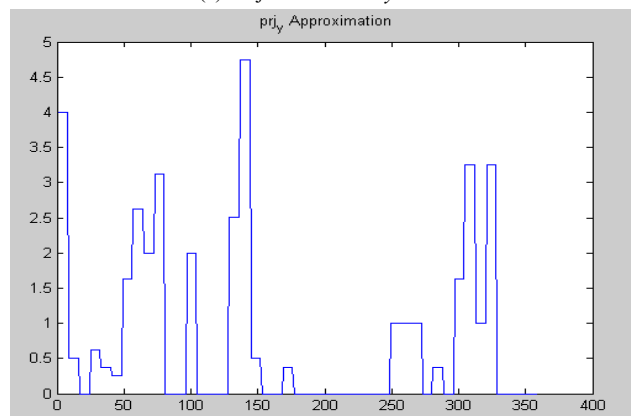
(b) Binary figure



(d) Projection on the x axis after wavelet denoising



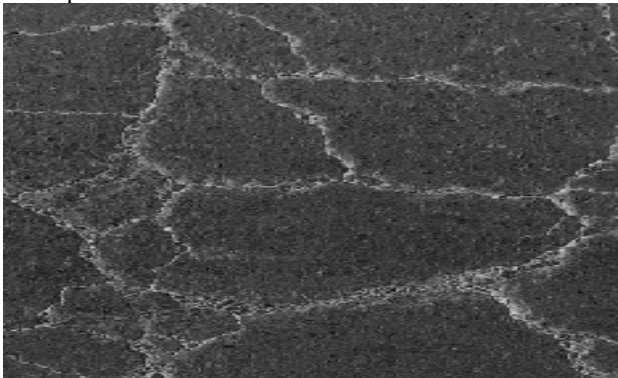
(e) Projection on the y axis



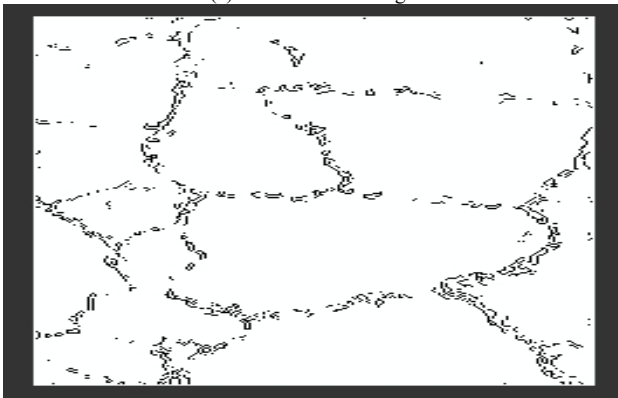
(f) Projection on the y axis after wavelet denoising

Fig.6. Projection of longitudinal cracks.

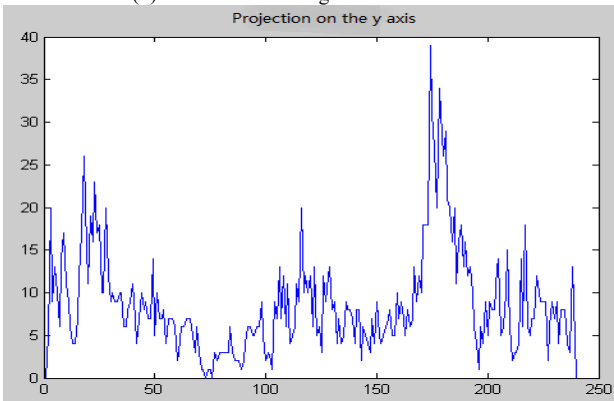
Fig.7 (a) presents an image of a meshed crack. As shown in Fig.7 (e) and Fig.7 (f), the projections of the x coordinates and y coordinates have at least three obvious peaks. However, simply relying on the projections cannot effectively distinguish between meshed and linear cracks. Other parameters are needed for the classification.



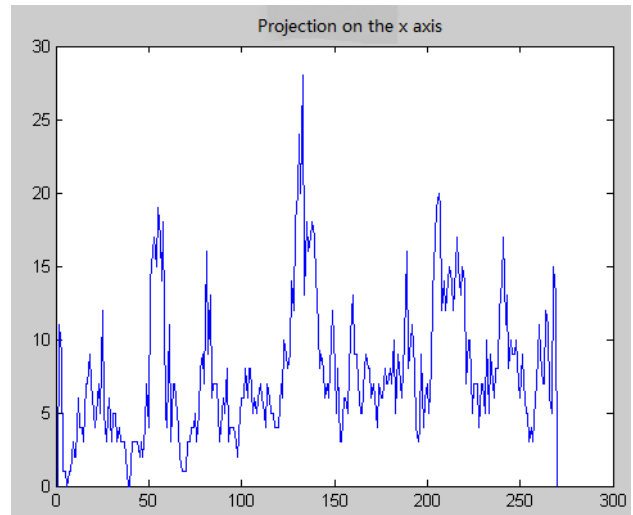
(a) Meshed crack image



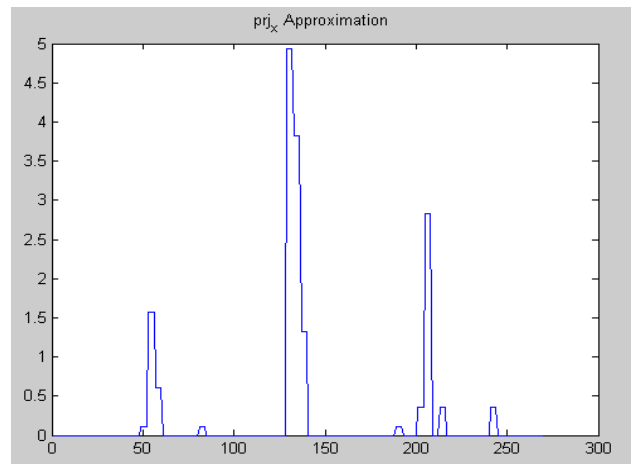
(b) Meshed crack image from binarization



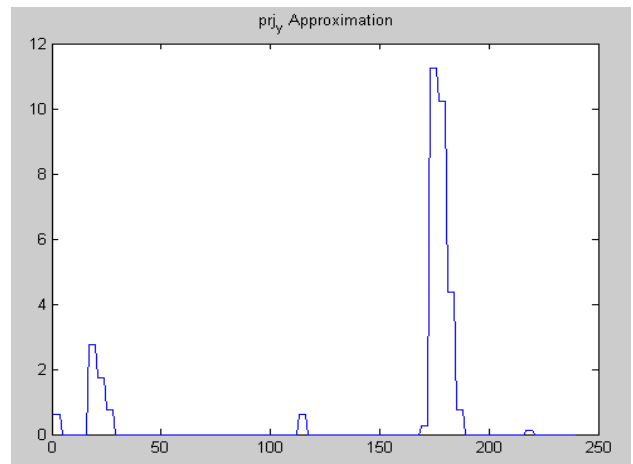
(c) Projection on the y axis



(d) Projection on the x axis



(e) X-axis projection after setting a threshold and wavelet denoising



(f) Y-axis projection after setting a threshold and wavelet denoising

Fig.7. Projection and wavelet denoising of a crack image

3.3 Multi-characteristic parameter classification algorithm for cracks on a bridge substructure

The crack types were further identified by combining many characteristic parameters of the bridge substructure's cracks. This method can help provide a scientific evidence for the maintenance of bridges.

3.3.1 Classification algorithm based on the number of pixels and the distribution density

The total pixel number (denoted by Sum) of the crack target is occupied by the different types of cracks varies considerably. Transverse, longitudinal, and other linear cracks often account for only a small part of the whole bridge image; therefore, the pixel number of the crack target per unit area is low. By contrast, reflective cracks occupy a large area of the image; thus, more pixels of the target are observable in the crack per unit area. Meshed cracks can be regarded a denser crack than the reflective cracks, and the pixel number of their crack target per unit area will be higher than that of the reflective cracks. Therefore, number of pixels per unit area can be used to reflect the type of crack to a certain extent.

The distribution density of the cracks was assumed to be p , and its value was based on Sum the ratio of the number of pixels in the crack region to the rectangle area S_r outside the crack area. In the actual segmentation algorithm, the rectangle area outside the crack area can be obtained directly from the most peripheral pixel points inside the crack area. However, the deviation of the distribution density obtained by this algorithm for the abovementioned calculation ratio p is extremely large. Hence, the algorithm needs to be improved. The improved algorithm is explicated in four steps.

Step 1: Obtain the geometric centroid coordinates x_{geo} and y_{geo} of the lower-structural cracks:

$$x_{geo} = \frac{1}{sum} \sum_{I(i,j) \neq 1} j \tag{5}$$

$$y_{geo} = \frac{1}{sum} \sum_{I(i,j) \neq 1} i \tag{6}$$

Step 2: Create an external rectangle. Set the center to $I(x_{geo}, y_{geo})$ and the border length to $2r+1$ (initial value $r=10$), then calculate the ratio of the total number of pixels to the total number of pixels (P) in the rectangle area of the image. When $P \leq 80\%$, proceed to **step 3**. Otherwise, skip to **step 4**.

Step 3: Set $r=r+10$, and repeat **step 2**.

Step 4: Calculate the distribution density of the bottom structure with $P = sum_r / (2r+1)^2$.

The results indicate that the distribution density of the linear cracks (transverse and longitudinal cracks) is relatively small, the distribution density of the reflective cracks is relatively large, and the density of the network cracks is the largest. Therefore, the distribution density of the pixels in the crack area can be used as one of the basis for judging the type of cracks. How the characteristic parameters of the crack image are calculated when the image required to be changed?

3.3.2 Addition of the Euler number to the classification algorithm

On the basis of previous discussion, the Euler number was introduced to retain the image characteristic when the image is subsequently changed into a two-dimensional bridge crack image. The Euler number [24] was represented by E , the number of connected objects was denoted by C , and the number of holes was denoted by H . Here, E corresponds

to the difference between C and H , as expressed by Formula 7.

$$E=C-H \tag{7}$$

For the binary bridge crack images, the ratio of the number of holes to the background area with edges was defined as H , including the area surrounded by pixels on the edge of a meshed cracks' target. For the cracks images without holes, the Euler numbers can be used to calculate the number of connectors or determine if the cracks are linear cracks. Euler numbers are calculated using adjacent pixels. The bridge crack images were divided into four and eight connections. The Euler numbers in the formulas for the four and eight connections differ from each other, as shown in Formulas 8 and 9:

Four connections:

$$E(4) = Q_1 - Q_3 + D_1 \tag{8}$$

Eight connections:

$$E(8) = Q_1 - Q_3 - D_2 \tag{9}$$

Among them, Q_1 , Q_3 , D_1 , and D_2 represent the four parameters for the Euler numbers, in which the arrangement pattern is set to $\left(\begin{bmatrix} 0 & 1 \\ 1 & 0 \end{bmatrix}, \begin{bmatrix} 0 & 1 \\ 1 & 1 \end{bmatrix}, \begin{bmatrix} 1 & 0 \\ 0 & 1 \end{bmatrix}, \begin{bmatrix} 0 & 1 \\ 1 & 0 \end{bmatrix} \right)$ in the binary images [23].

The procedure for calculating the Euler number can be simplified by adopting a new formula. In particular, the scanning of an image from top to bottom is only performed once, and only two lines of data were used for the scan, indicating a reduction in memory capacity. Formulas 8 and 9, representing the four and eight connections, were unified and substituted by Formula 10:

$$E = \sum_{m=1}^M \sum_{k=0}^K (1 - V_{mk}) \tag{10}$$

Where v_{mk} represents the upper-phase field corresponding to the m -th row and the k -th segment. In the image, when $k=0$ and the line M has no graph section, $v_{mk}=1$ indicates that the line cannot be calculated with the Euler number. The difference between the Euler number with four connections and that with eight connections can be attributed to the width of the preceding line corresponding to the k -th segment; that is, the eight connections have more pixels than the four connections in the left and right parts.

The analytical findings on the relationship among Euler number, number of holes, and types of crack for a bridge image are as follows. First, the number of holes represents a linear crack when $H \leq 1$, whereas it represents a meshed crack when $H \geq 1$. Second, the number of holes per unit area in the reflective crack image is much smaller than that in the meshed crack image. Finally, by combining the projection variances Q_3 and Q_1 , pixel distribution density P , and holes number H , the four kinds of cracks (transverse, longitudinal, meshed, and reflective cracks) can be classified effectively.

4. Result Analysis and Discussion

In this section, the proposed algorithm for bridge substructure will be tested. The method with canny has been selected for comparison with the proposed approach. All the experiments have been performed on an Intel® Celeron® CPU 550 machine (3.2 GHz, 4 GB memory). The operating system is MS Windows 10 and the program compiler is VC++ 6.0.

4.1 Experimental result

The pixel distribution density P , projection variances Q_s and Q_r , and hole number H of the image were calculated using the OpenCV dynamic link library function in the Visual C++ 6.0 development environment. A BP neural network classifier was also employed to classify the substructure's cracks. The classifier used a gradient descent algorithm to select 50 radial base nodes, 4 input nodes, and 4 output nodes. The input vector of the classifier was (Q_s, Q_r, P, H) , while the input parameter was $(01, 10, 11, 00)$. A total of 280 character vectors were obtained from the 280 crack images. The target error was set to 0.02, and the learning process converged after 3000 experiments. Then, the software calculation of the crack widths was compared with the microscopic measurement (shown in Table 1). The classification results with canny operator were also compared. The classification results of this study are shown in Table.2, Fig.9 and Fig.10.

As shown in Table.2, Fig.8 and Fig.9, the classification algorithm used in this study can effectively identify the transverse, longitudinal, reflective, and meshed cracks. Except for the classification accuracy of the meshed crack, the classification accuracies of the other cracks are higher than those that used canny operator. Thus, our proposed

method can meet the requirements of crack classification accuracy in practical engineering.

4.2 Error analysis

The error was related to the intercept position, the size of the shooting data, the size of the threshold, the size calculated by software, and the error brought by human eye estimation when measuring the size by microscope.

(1) When the distance is 6800 mm, the calculation errors (minimum, maximum, and average values) for the crack images of the bridge pier are -1.478955, 0.02109, and 0.00817 mm, respectively.

(2) When the shooting distance above the bridge pier's cracks is 11138 mm, the calculation error is within the effective range, and the algorithm can be regarded effective. The actual data found in the part of the algorithm error are relatively large. The main reason is that the pier cracks were microscopically observed for their individual position estimate values, but the actual crack situation is complex. Given the existence of numerous interference factors, an estimation error analysis with the human eye cannot completely reflect the actual crack widths.

(3) The cracks' minimum values derived from the software calculation are extremely close to the values listed via the actual human eye observation.

(4) The calculation error results are smaller compared with those of a bridge pier photograph found in the wall crack image of a highway-testing center. This finding can be explained by a number of reasons. For instance, the area has good lighting conditions, the walls are relatively clean, the noise effect is small, and the grayscale distribution has an average value. These settings are beneficial to the realization of the algorithm.

Table 1. Comparison between software calculation and microscopic measurement of crack widths (partial data)

Interception location	Photographic distance (mm)	Threshold selection	Software calculation size (mm)	Number of pixels (pixel)	Microscopic measurements (mm)	Mean error analysis (mm)
A	10744	[120 140]	Minimum: 0.191603 Maximum: 0.988130 Average: 0.336538	Minimum: 1.000000 Maximum: 5.157169 Average: 1.756431	Eye estimates: 0.40	-0.063462
B	10744	[120 150]	Minimum: 0.191603 Maximum: 0.789727 Average: 0.400842	Minimum: 1.000000 Maximum: 4.121677 Average: 2.092040	Eye estimates: 0.1-0.25	0.150842-0.300842
A	8840	[110 125]	Minimum value: 0.174693 Maximum: 0.960256 Average: 0.356832	Minimum: 1.000000 Maximum: 5.496837 Average: 2.042631	Eye estimates: 0.35	0.06832
B	8840	[115 125]	Minimum: 0.174693 Maximum: 0.912908 Average: 0.366934	Minimum: 1.000000 Maximum: 5.225798 Average: 2.100456	Eye estimates: 0.35	0.0562908
A	6800	[110 125]	Minimum: 0.148884 Maximum: 2.265703 Average: 1.728955	Minimum: 1.248528 Maximum: 19.000000 Average: 14.498877	Eye estimates: 0.25	-0.02109

B	6800	[120 130]	Minimum: 0.119248 Maximum: 0.480696 Average: 0.228910	Minimum: 1.000000 Maximum: 4.031075 Average: 1.919621	Eye estimates: 0.25	0.00817
A	11138	[110 125]	Minimum: 0.198831 Maximum: 1.926243 Average: 0.714046	Minimum: 1.000000 Maximum: 9.687818 Average: 3.591210	Eye estimates: 0.25	0.464046
B	11138	[100 120]	Minimum: 0.198831 Maximum: 1.585276 Average: 0.677777	Minimum: 1.000000 Maximum: 7.972961 Average: 3.408800	Eye estimates: 0.25	0.427777

Table 2. Crack image classification result

Number of images/crack type	Transverse cracks (01)	Longitudinal cracks (10)	Reflective cracks (11)	Meshed cracks (00)
Total number of images	89	65	68	58
Correct classification number with the Canny operator	65	51	50	49
Classification accuracy with Canny operator recognition	73%	79%	74%	84%
Number of correct classifications in this study	76	52	52	46
Accuracy of this study	85%	82%	78%	79%

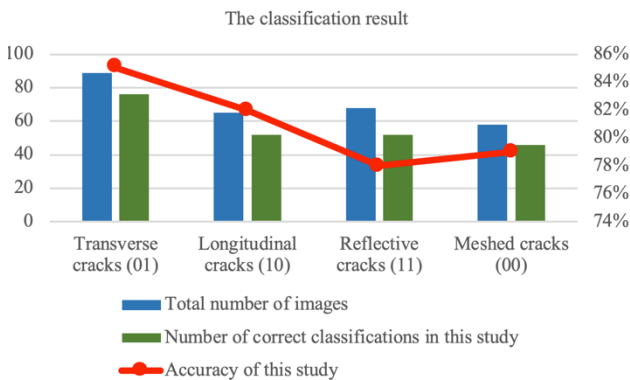


Fig. 8. Classification effects of the four types of cracks.

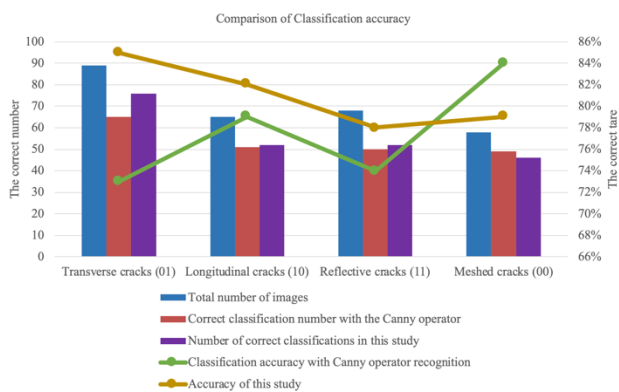


Fig.9. Comparison of classification results between the two algorithms.

5. Conclusions

This study extracted the projection variances Q_x and Q_y , pixel distribution density P , number of holes H , and the Euler number of the crack images to accurately identify the bridge cracks, improve the classification precision of the bridge cracks, and provide a highly scientific basis for

bridge maintenance. By using the above parameters, a crack classification algorithm for the lower part of a bridge structure was constructed. Then, the classification experiment was verified by employing the BP neural network. The conclusions of this research are as follows.

(1) The projection and wavelet denoising algorithms can be used to distinguish between the linear cracks (longitudinal and transverse fractures) and the meshed cracks. For a standard transverse crack, the projection variance of the x axis is markedly larger than that of the y axis. For a standard longitudinal crack, the projection variance of the y axis is considerably larger than that of the x axis.

(2) Different crack distribution densities were employed to distinguish between the meshed cracks and the reflective cracks. The linear cracks (transverse and longitudinal cracks) have a relatively small distribution density; the reflective cracks have a relatively large distribution density; and the network cracks have the largest distribution density.

(3) The Euler number was introduced to retain the image's characteristics when the image needs to be expanded. The number of holes in the image is taken as the parameter to further distinguish the crack types. For the linear cracks, the number of holes is $H \leq 1$. For the reflective and network cracks, the number of holes is $H \geq 1$. Moreover, the number of holes H per unit area in the reflective crack image is much smaller than that in the meshed crack image.

(4) The BP neural network was further combined with the above parameters to realize the accurate classification of the transverse, longitudinal, and reflective cracks. The effectiveness of the algorithm has been verified by the experiments. The experimental results show that the classification algorithm can effectively identify the transverse, longitudinal, reflective, and meshed cracks, and the accuracy is better than the method using the canny operator.

The experimental results show that the algorithm is accurate and has a reference value for the effective

maintenance of bridges. However, as the number of crack images collected in this study is small, the number and algorithm of the crack images may need to be modified in future research. Moreover, when calculating for the eigenvalues, the classification algorithm assumes that an image has only a single substructure crack target. Although this assumption is true for most images, it is not rigorous theoretically. Knowing how to automatically determine the number of substructure cracks in images and how they can be identified separately will be the next research direction for the algorithm.

Acknowledgements

This work was supported by the Special Scientific Research Project of the Shaanxi Provincial Department of Education

(17JK0278), Weinan Normal University Reform Research Project (JG201926), Professional Master Degree Construction Project (18TSXK06), and Weinan Normal University Scientific Research Project (18YKS14), Chinese Ministry of Education Industry-school Cooperative Education Project (201802314001, 201901291014)

This is an Open Access article distributed under the terms of the Creative Commons Attribution License



References

- Huang, Y.X., Xu, B.G., "Automatic inspection of pavement cracking distress". *Electron Imaging*, 15(1), 2006, pp.56-68.
- Xiao, J., Huang, X.H., Ang, K., "Application of template matching based on Hu moment on target recognition in micro-vision". *Journal of Huazhong University Science and Technology. (Natural Science Edition)*, 43(1), 2015, pp.148-151.
- Lins, R.G., Givigi, S.N., "Automatic crack detection and measurement based on image analysis". *IEEE Transactions on Instrumentation and Measurement*, 65(3), 2016, pp.583-590.
- He, Y.Q., "The application research of computer vision in bridge health monitoring". *Journal of Communication and Computer*, 7(2), 2010, pp.6-8.
- Wang, W.X., Wang, M.F., Li, H.X., Zhao, H., Wang, K.V., He, C.T., Wang, J., Zheng, S.F., Chen, J.B., "Pavement crack image acquisition methods and crack extraction algorithms: a review". *Journal of Traffic and Transportation Engineering*, 6(6), 2019, pp.535-556.
- Chen, C.J., Pai, T.W., Cheng, M., "A support vector machine approach for truncated fingerprint image detection from sweeping fingerprint sensors". *Sensors*, 15(4), 2015, pp.7807-7822.
- Cao, Y.F., Zhao, Y.J., "Research on intelligent image recognition technology based on ga-bp neural network". *Applied Laser*, 37(1), 2017, pp.139-141.
- Linda, C.H., Jiji, G.W., "Crack detection in X-ray images using fuzzy index measure". *Applied Soft Computing*, 11(4), 2011, pp.3571-3579.
- Yao, B., He, L.F., Kang, S.Y., Zhao, X., Chao, Y.Y., "Binary image eight adjacency Euler algorithm based on the graph theory". *Journal of Naval University of Engineering*, 28(5), 2016, pp.37-40.
- Li, N., Xu, Y.F., Jia, P.T., "Method for quickly identifying bridge cracks based on second order moment & gray difference". *Computer Applications and Software*, 36(5), 2017, pp.216-219.
- Zhao, W.H.D., Cheng, B., Jiang, Sh. Y., "An adaptive multiscale approach for identifying multiple flaws based on XFEM and a discrete artificial fish swarm algorithm". *Computer Methods in Applied Mechanics and Engineering*, 339(9), 2018, pp.341-357.
- Zhu, R., Xiao, N., "Morphological measurement of cracks in geotechnical microscopic images". *Acta Microscopica*, 28(5), 2019, pp.1357-1367.
- Jovisa, Z., Kaoru, H., Dragan, D., Aktas, M.A., "On a 3D analogue of the first Hu moment invariant and a family of shape ellipsoidness measures". *Machine Vision and Applications*, 27(1), 2016, pp.129-144.
- Gishkori, S., Mulgrew, B., "Pseudo-Zernike moments based sparse representations for SAR Image Classification". *IEEE Transactions on Aerospace & Electronic Systems*, 55(2), 2019, pp. 1037-1044.
- Qian, B., Tang, Z.M., Xu, W., "Pavement crack detection based on improved tensor voting". In: *The 9th International Conference on Computer Science & Education (ICCSE 2014)*, Vancouver, Canada: IEEE, 2014, pp.22-24.
- Xu, D.L., Du, L., Liu, H.W., Wang, P.H., "Bayesian classifier for sparsity-promoting feature selection". *International Journal of Pattern Recognition & Artificial Intelligence*, 29(6), 2015, pp.1-28.
- Bar, H., Booth, J., Wells, M.T., Liu, K.Y., "Facilitating high-dimensional transparent classification via empirical Bayes variable selection". *Applied Stochastic Models in Business & Industry*, 34(6), 2018, pp.949-961.
- Jimenez, A.A., Garcia, M.F.P., Moraleda, V.B., Gomez, M.C.Q., "Linear and nonlinear features and machine learning for wind turbine blade ice detection and diagnosis". *Renewable Energy: An International Journal*, 132(3), 2019, pp.1034-1048.
- Sakshi, R.K., "A Computationally Efficient Weight pruning algorithm for artificial Neural Network classifiers". *Arabian Journal for Science & Engineering*, 43(12), 2018, pp.6787-6799.
- Zhao, X.L., Zhang, Y.L., Zhang, T., Zou, X.M., "Channel splitting Network for single MR Image super-resolution". *IEEE Transactions on Image Processing*, 28(11), 2019, pp.5649-5662.
- Wang, L.P., Gao, R.Z., Zhang, J.J., Wang, E.C., "Crack detection of concrete pavement based on convolutional Neural Network". *Computer Science*, 46(11), 2019, pp.586-588.
- Zhao, Y.T., Chen, Q.K., Ji, L.N., Liu, B.C., "Connected image labeling algorithm for binary images based on CUDA". *Journal of Computer-Aided Design & Computer Graphics*, 29(1), 2017, pp.72-78.
- Kim, H.J., Ahn, E.J., Cho, S.J., Shin, M.G., Sim, S.H., "Comparative analysis of image binarization methods for crack identification in concrete structures". *Cement and Concrete Research*, 99(9), 2017, pp.53-61.
- He, L.F., Chao, Y.Y., Kenji, Suzuki, K., "An Algorithm for connected-component labeling, hole labeling and Euler number computing". *Journal of Computer Science and Technology*, 28(3), 2013, pp.468-478.